Published in final edited form as:
Bioconjug Chem. 2010 December 15; 21(12): 2197–2204. doi:10.1021/bc100180q.

A Mixed Stimuli-Responsive Magnetic and Gold Nanoparticle System for Rapid Purification, Enrichment, and Detection of Biomarkers

Michael A. Nash, **Paul Yager**, **Allan S. Hoffman**, and **Patrick S. Stayton***
Department of Bioengineering, University of Washington, Seattle, WA 98195

Abstract

A new diagnostic system for the enrichment and detection of protein biomarkers from human plasma is presented. Gold nanoparticles (AuNPs) were surface-modified with a diblock copolymer synthesized using reversible addition fragmentation chain transfer (RAFT) polymerization. The diblock copolymer contained a thermally-responsive poly(N-isopropylacrylamide) (pNIPAAm) block, a cationic amine-containing block, and a semi-telechelic PEG_2-biotin end group. When a mixed suspension of 23 nm pNIPAAm-modified AuNPs was heated with pNIPAAm-coated 10 nm iron oxide magnetic nanoparticles (mNPs) in human plasma, the thermally-responsive pNIPAAm directed the formation of mixed AuNP/mNP aggregates that could be separated efficiently with a magnet. Model studies showed that this mixed nanoparticle system could efficiently purify and strongly enrich the model biomarker protein streptavidin in spiked human plasma. A 10 ng/mL streptavidin sample was mixed with the biotinylated and pNIPAAm modified AuNP and magnetically separated in the mixed nanoparticle system with pNIPAAm mNPs. The aggregates were concentrated into a 50-fold smaller fluid volume at room temperature where the gold nanoparticle reagent redissolved with the streptavidin target still bound. The concentrated gold-labeled streptavidin could be subsequently analyzed directly using lateral flow immunochromatography. This rapid capture and enrichment module thus utilizes the mixed stimuli-responsive nanoparticle system to achieve direct concentration of a gold-labeled biomarker that can be directly analyzed using lateral flow or other rapid diagnostic strategies.

INTRODUCTION

Diagnostic testing is expanding from centralized hospital labs to more distributed settings in both the developed and developing worlds. A current dominant point-of-care diagnostic test format is the lateral flow immunoassay (LFIA[1]) (1), which relies on capillary wicking of fluids through porous nitrocellulose strips. Such tests typically rely on the specific binding between gold-labeled biomarkers with capture antibodies immobilized at the test line of the solid phase. Current devices possess many desirable features, such as being rapid, inexpensive, portable, and easy to use. However, they suffer from a limitation in sensitivity related to the small sample volume (2) that limits the biomarker repertoire to those at relatively higher blood and plasma concentrations (3). These limitations have created a need

*Corresponding author. Patrick S. Stayton, Ph.D. University of Washington, Department of Bioengineering, Box 355061, Seattle, WA 98195, Tel: (206) 685-8148, Fax: (206) 685-8526, stayton@u.washington.edu.

Supporting Information Available: Figure S1: Refractive index GPC traces of mCTA and diblock copolymers, Figure S2: Proton NMR spectroscopy of the diblock copolymer, Figure S3: Quantitation of biotinylation efficiency by HABA assay, Figure S4: Time-lapse images of mNP/AuNP co-aggregation and separation process, and Figure S5: Lateral flow strip images and linescans from PfHRP2 biomarker assay. This material is available free of charge via the internet at http://pubs.acs.org.

[1]LFIA: Lateral flow immunoassay

for rapid and simple sample processing strategies for purifying and enriching biomarkers in a form that could then be applied directly to the existing lateral flow tests or other types of newly developed rapid tests.

Magnetic separation and enrichment strategies represent one of the most common methods for biomarker purification and separation. We have recently described a stimuli-responsive magnetic nanoparticle system (4,5) that circumvents one of the primary limitations of magnetic separations. This nanoparticle system allowed the use of very small magnetic nanoparticles that optimize biomarker binding, while still allowing rapid magnetophoretic separation of thermally-aggregated nanoparticle-biomarker complexes. This system was useful for purification and concentration, but additional steps of biomarker release and gold labeling for optimized visual detection would be required in lateral flow or flow-through tests. AuNPs have a long history as optical labels in immunoassay and biodetection (6–13) due to their large extinction coefficients ($>10^9$ $M^{-1}cm^{-1}$) in the visible range, and enhanced electric near-fields at the particle surface. While one potential solution to simplifying this system would be to use a stimuli-responsive core-shell Au/mNP system (14–19), we present here the finding that mixed stimuli-responsive AuNPs and mNPs co-aggregate efficiently.

This system thus achieves rapid magnetic separation of the Au-labeled biomarker in a simple mixture of separate stimuli-responsive nanoparticles where each can be optimized independently. Stimuli-responsive polymers such as poly(N-isopropylacrylamide) (pNIPAAm) with “smart” phase-transition properties have been shown to enhance the capture/separation capabilities of immunoassays (20). The work presented herein shows that the pNIPAAm-mNPs can capture the pNIPAAm-AuNPs through a co-aggregation mechanism, so that the thermally-triggered and high-efficiency enrichment of the Au-labeled biomarker to be used in lateral flow is achieved in one step. To our knowledge this is the first time the general strategy of stimuli-responsive phase separations has been applied to synergistically direct co-aggregation of nanoparticles with different compositions and functions, i.e. magnetic nanoparticles aggregated with a gold nanoparticle labeling reagent. The size of the co-aggregates are large enough to rapidly magnetophorese toward the applied magnet. This strategy for purification and enrichment might also circumvent the high dose “hook” effect that can occur when excess sample antigen occupies all of the binding sites on the solid-phase, preventing the gold-labeled antigen from binding (21). This confounds LFIAs because it results in lower signal strength at high antigen concentrations. Magnetic separation eliminates the high dose “hook” effect because only antigen molecules bound to a label are separated and applied to the flow strip. Magnetic separation/enrichment of the gold-labeled biomarkers from larger plasma volumes could therefore not only increase the sensitivity of LFIA, but could also eliminate sample-matrix-derived interferences.

EXPERIMENTAL PROCEDURES

Materials and Suppliers

N,N-dimethylaminoethylacrylamide (DMAEAm[2]; Monomer, Polymer, & Dajac Labs) was twice distilled through a short path prior to use. NIPAAm (Sigma, 97%) was recrystalized from hexanes prior to use. 2,2-Azobis(2-methylpropionitrile) (AIBN; Aldrich, 98%) was recrystalized from methanol. The RAFT chain transfer agent 4-Cyano-4-(dodecylsulfanylthiocarbonyl)sulfanyl pentanoic acid (DCT) was synthesized as described in the literature (22). 2-(Dodecylsulfanylthiocarbonylsulfanyl)-2-methylpropionic acid (DMP) was a gift from Noveon. Dioxane (EMD, 99%), dimethylformamide (DMF; EMD,

[2]DMAEAm: N,N-dimethylaminoethylacrylamide

99.8%), dichloromethane (DCM; EMD, 99.8%), pentane (J.T. Baker, 99%), tetraglyme (Aldrich, 99%), methanol (MeOH; EMD, 99.9%), tetrahydrofuran (THF; Mallinckrodt, 99.8%), N,N′-dicycohexylcarbodiimide (DCC; Fluka, 99%), N-Hydroxysuccinimide (NHS; Fluka, 97%), $HAuCl_4$ (Aldrich, 99.99%), $Fe(CO)_5$ (Aldrich, 99.9%), and D-biotin (Aldrich, 99%) were used as received. Cellulose ultrafiltration membranes for AuNP purification were from Millipore (regenerated cellulose, 44.5 mm diameter, NMWL 100,000, Cat No: 14422AM) and PD-10 desalting columns were from GE Healthcare. NH_2-PEG_2-biotin, HABA biotin quantitation kit, and dialysis membranes (7 & 20 kDa MWCO) were purchased from Pierce. Streptavidin labeled with Alexafluor® 750 (SA-750 streptavidin) was purchased from Invitrogen. Purified rabbit polyclonal anti-streptavidin IgG was purchased from Abcam (Product No. Ab6676). 1x phosphate buffered saline packets (1x PBS; 10 mM phosphate, 138 mM NaCl, 2.7 mM KCl, pH 7.4 at 25 °C) were purchased from Sigma. Human rediscovered plasma in disodium EDTA (Valley Biomedical Inc., product No. HP1051) was centrifuged at 1000× g for 30 minutes, and filtered through GDX graded syringe filters (Whatman) prior to use. Magnets were NdFeB, 5 cm × 1.27 cm × 0.63 cm, Br max =12.1 kGauss (Force Field Magnets.com). Nitrocellulose LFIA membranes were Millipore HiFlow Plus 180. Zymed non-specific membrane blocking solution was purchased from Invitrogen.

Polymer Synthesis

RAFT polymerization was carried out using previously published procedures with slight modification (4). A homo-pNIPAAm polymer with a target molecular weight of 15 kDa was polymerized by dissolving in a round bottom flask 2 grams (17.7 mmol) of NIPAAm, 54 mg (0.134 mmol) of DCT, and 2.2 mg (13.4 μmol) of AIBN in 4 grams p-dioxane. The flask was purged with N_2 for 30 minutes and heated at 60 °C for 12 hours, followed by precipitation into pentane. The product was dried under vacuum, dialyzed against DI water at 4 °C, and freeze-dried. A 5 kDa homo-pNIPAAm for use in mNP synthesis was prepared by polymerization in a round bottom flask containing 2 grams (17.7 mmol) of NIPAAm, 143.3 mg (0.4 mmol) of DMP, 6.66 mg (40.5 μmol) of AIBN, and 4 grams of p-dioxane. Precipitation and purification was carried out identically as for the 15 kDa homo-pNIPAAm. Diblock extension was performed by dissolving in a round-bottom flask 1.32 g (83 μmol) of the ~15 kDa homo-pNIPAAm mCTA, 0.2258 g (1.59 mmol) of DMAEAm, 0.18 g (1.59 mmol) of NIPAAm, 1.4 mg (8.3 μmol) of AIBN in 8 mL of MeOH. This resulted in a [DMAEAm]:[NIPAAm]:[mCTA]:[initiator] ratio of 18:18:1:0.1. The flask was purged with N_2 for 30 minutes, followed by heating at 60 °C for 18 hours. The MeOH was removed by rotary evaporation, and the product was dissolved in 5 mL of THF, and precipitated thrice into pentane. The precipitate was dried under vacuum, dissolved in DI water, purified by PD-10 desalting column, and freeze-dried.

Polymer Analysis

Polymers were characterized using GPC performed on an Agilent 1200 series liquid chromatography system, equipped with TSKgel alpha 3000 and TSKgel alpha 4000 columns (TOSOH biosciences). The mobile phase was LiBr (0.01 M) in HPLC grade DMF at a flow rate of 1 mL/min. MALS data were obtained on a miniDAWN TREOS (Wyatt Technologies Corp.) with 658 nm laser source, and three detectors at 45.8°, 90.0°, and 134.2°. The instrument calibration constant was $5.746*10^{-5}$ $V^{-1}cm^{-1}$. Refractive index was measured using an Optilab Rex detector (Wyatt Technologies Corp.). The dn/dc value for the homo-pNIPAAm macro-chain transfer agent (mCTA) was determined under the assumption of 100% mass recovery. The dn/dc value for the diblock copolymer was determined by injecting polymer samples at known concentrations into the RI detector post-column. The dn/dc value was then calculated using linear regression with the Astra 5.3.4.14 data analysis software package (Wyatt Technologies Corp.). ^{1}H-NMR (300 MHz.) spectroscopy in $CDCl_3$

was obtained on a Bruker AV300. Nanoparticle absorption was measured on a Hewlett Packard 8453 diode array extinction spectrophotometer with quartz cuvette sample holder. TEM was performed on a Technai G2 F20 200 kV microscope. Absorbance and fluorescence measurements were made using a 96-well microplate reader (Tecan).

Biotinylation of Diblock Copolymer

NHS activation of the diblock copolymer was performed by dissolution of 1.29 g (73 μmol) of polymer, 76 mg (372 μmol) of DCC, and 42 mg (365 μmol) of NHS in 7 mL of DCM. The reaction proceeded for 24 hours at 22 °C, at which time an additional 76 mg of DCC and 42 mg of NHS were added. The reaction was allowed to proceed for an additional 24 hours. The mixture was precipitated into pentane and dried under vacuum. The NHS-activated polymer was then mixed with 100 mg (266 μmol) of NH_2-PEG_2-biotin in 3 mL of DMF. The conjugation proceeded for 48 hours at 22 °C and was precipitated into diethyl ether. The product was dried under vacuum, dissolved in DI water, filtered through a 0.2 μm filter, and obtained through PD-10 column purification, and freeze-drying. Biotinylation efficiency was estimated using a commercially available HABA biotin quantification kit carried out according to manufacturer's instructions.

Nanoparticle Synthesis and Characterization

Citrate-stabilized colloidal gold was prepared according to the literature (23). All glassware was cleaned with aqua regia, thoroughly rinsed with DI water, and dried in an oven before use. 150 mL of 0.1 mg/mL $HAuCl_4$ was brought to a boil in a round bottom flask. 1.76 mL of 10 mg/mL sodium citrate in DI water was added. The reaction was boiled under reflux for 30 minutes and cooled to room temperature. The pH was raised to 8 by addition of 0.1 M NaOH. Next, 1.2 mL of a 10 mg/mL solution of 17.7 kDa biotinylated diblock copolymer in DI water was added. The flask was purged with N_2 for 45 minutes. The gold sol was then sealed and stirred at 22 °C for 24 hours in darkness, after which 1 g of NaCl was added, followed by an additional 24 hours of stirring. The particles were then concentrated under 35 psi of N_2 using a membrane ultrafiltration system with a cellulose membrane (MWCO=100,000 kDa). The polymer-modified gold nanoparticles (AuNPs) were washed off of the membrane with 3 mL of PBS buffer. The AuNPs were stored in PBS at 4 °C under N_2 for up to 4 months and used for further streptavidin binding/enrichment studies.

Magnetic nanoparticles (mNPs) coated with 5 kDa homo-pNIPAAm (without biotin) were synthesized as previously described (4,5), with slight modification. Briefly, the 5 kDa homo-pNIPAAm was dissolved in tetraglyme (3.6 mM) at 100 °C. Iron pentacarbonyl ($Fe(CO)_5$) was iltered through a 0.45 μm syringe filter prior to use. 4 μL $Fe(CO)_5$ per mL of tetraglyme was added. After 10 minutes of stirring, the temperature was raised to 180 °C for 5 hours. The reaction was cooled, and the mNPs obtained by precipitation into pentane, drying under vacuum, dialysis against DI water at 4 °C, and freeze-drying. The mNPs were then dissolved in DI water at 50 mg/mL and stored at 4 °C for up to 3 months. TEM samples were prepared by dissolving particles in DI water (1 nM for the AuNPs, and 3 mg/mL for the mNPs). Particle solutions were aerosolized onto carbon-stabilized formvar-coated copper grids (Ted Pella) using a spray bottle.

Magnetic Enrichment of Alexafluor®-750-Labeled Streptavidin

Pooled human plasma was diluted with an equal volume of 2x PBS (20 mM phosphate, 276 mM NaCl, 5.4 mM KCl, pH 8.0). Alexafluor®-750-labeled streptavidin (AF-750 streptavidin) was spiked into the 50% human plasma at a concentration of 5 nM. Stock solutions of the nanoparticle reagents were added to achieve final concentrations of 3 nM and 2 mg/mL for the AuNPs and mNPs, respectively. 8 kDa homo-pNIPAAm free polymer was added to a final concentration of 2 mg/mL. As a negative control, 1 μM free biotin was

included in the plasma dilution buffer. 100, 250, or 500 μL of the 5 nM AF-750 streptavidin in 50% human plasma was added to Eppendorf® tubes. Samples were incubated for 15 minutes with orbital shaking (400 rpm) inside an aluminum tube-holder equilibrated in an incubator set to 45 °C. This was followed by incubation of the sample tubes in close contact with neodymium iron boron magnets for 15 minutes at 45 °C using an in-house fabricated magnet holder. Next, the supernatant was discarded with a pipette, and the precipitate that had been captured along the side of the tube was resuspended into 10 μL of 1x PBS pH 6.0 buffer at 4 °C. Fluorescence of the AF-750 streptavidin (λ_{ex}=752 nm, λ_{em}=776 nm), and absorbance of the AuNPs at 520 nm were measured using a fluorescence/absorbance microwell plate reader (Tecan).

LFIA Device Fabrication

Rabbit polyclonal anti-streptavidin IgG was deposited at 3 mg/mL onto HiFlow 180 nitrocellulose assay membranes using an in-house fabricated protein striping system. The membrane was diced into rectangles measuring 16 × 3 mm using a CO_2 laser system (Universal Laser Systems). The strips were submerged in goat protein non-specific blocking solution (Zymed) for 30 minutes, followed by drying in a vacuum desiccator overnight. The strips were then applied to adhesive coated mylar substrates measuring 48 × 3 mm. An absorbent pad (35 × 3 mm) was placed at the distal end of the flow strip to drive capillary wicking of the fluids. The length of the overlap between the assay membrane and the absorbent pads was 3 mm. LFIA strips were stored in a desiccator at 23 °C and used within one week.

Effect of Streptavidin Dose on LFIA Signal

200 μL samples of 50% human plasma containing variable amounts of non-fluorescent streptavidin, from 50 ng/mL to 0 ng/mL, were prepared. The AuNPs, mNPs, and 8 kDa homo-pNIPAAm were added to achieve final concentrations of 3 nM, 2 mg/mL, and 2 mg/mL, respectively. Heating, magnetic separation, and removal of the supernatant were performed as described in the fluorescent capture study (see above). The magnetically captured particle aggregates were resuspended into 10 μL of 1x PBS pH 6.0 at 4 °C. 10 μL droplets of the captured protein/particle mixture were deposited into wells of a 96-well plate. LFIA strips were placed into the droplets, which completely wicked into the strips within 5–6 minutes. The membranes were then transferred to wells containing PBS pH 6.0 rinse buffer. The buffer rinse was allowed to proceed for 20 minutes, or until the absorbent pad was saturated. Imaging of the developed strips was performed using a digital camera (Canon SD400) on digital macro setting. Strips were illuminated from behind at an oblique angle using a white light source, and the transmission images were quantified by image analysis. All samples were run in triplicate on three separate LFIA strips, and imaged under identical lighting conditions.

Image analysis was performed using Image J software. The background-corrected mean pixel intensity of the green channel in the RGB images was measured from a region of interest encompassing the leading edge of the antibody binding patch.

Effect of Increasing Sample Volume on LFIA Signal

10 ng/mL of streptavidin in 50% human plasma was prepared. Stock solutions of the nanoparticle/polymer reagents were added to achieve final concentrations of 3 nM, 2 mg/mL, and 2 mg/mL for the AuNPs, mNPs, and 8 kDa homo-pNIPAAm free polymer, respectively. The stock protein/particle solution at a fixed streptavidin concentration (10 ng/mL) was divided into aliquots of 100, 200, 300, 400, or 500 μL. Each sample tube was processed as described above. The captured aggregates were resuspended into 10 μL of 1x PBS pH 6.0 buffer at 4 °C. 10 μL droplets of the concentrated particle mixture were run on

the LFIA strips following the protocol described for the dose-response experiment (see above).

RESULTS

System Design

The bioseparation/enrichment system consists of a mixture of magnetic and gold nanoparticles, each with a “smart” polymer coating. Gold nanoparticles (~25 nm diameter) were modified with a biotinylated amine-containing diblock copolymer, and magnetic nanoparticles (~10 nm diameter) were synthesized directly with a homo-pNIPAAm polymer surface coating. When mixtures of these two particle types were heated above the polymer LCST, the particles co-aggregated driven by hydrophobic interactions between the collapsed polymers. 8 kDa homo-pNIPAAm (2 mg/mL) was added to the particle mixture to facilitate mNP and AuNP cross-aggregation. The aggregates contained both magnetic (iron oxide) and gold aggregates with a strongly enhanced magnetophoretic mobility that allowed them to be rapidly co-separated in an applied magnetic field gradient. The separation mechanism is depicted in Figure 1. By resuspending the magnetically captured particle aggregates into a smaller volume of fluid, the gold-labeled model target biomarker streptavidin could be concentrated many fold. The enriched gold-labeled target protein was then analyzed and visualized with an anti-streptavidin immunochromatographic flow strip.

Polymer synthesis and characterization

Polymer synthesis was carried out using two thermally-initiated RAFT polymerizations. The target molecular weight of the first RAFT polymerization was 15 kDa. A [NIPAAm]:[CTA]:[Initiator] ratio of 132:1:0.1 was used in p-dioxane. The homo-pNIPAAm product ((1) in Figure 2) was purified and analyzed. GPC showed the polymer had M_n=15.7 kDa, polydispersity index (PDI)=1.01, and dn/dc of 0.074. ^{1}H- NMR analysis confirmed the NIPAAm chemical shifts, with peaks at δ (ppm)=1.15 (s, R-CO-NH-CH-($C\underline{H}_3$)$_2$) and at δ (ppm)=4.00 (s, R-CO-NH-C$\underline{H}$-(CH_3)$_2$). These two peaks had an integrated peak area ratio of ~6:1, consistent with the proton ratio in the NIPAAm monomer.

Diblock extension was performed using the 15.7 kDa homo-pNIPAAm as a macro-chain transfer agent (mCTA). The mCTA was chain extended with a short random copolymer block of NIPAAm-co-DMAEAm. [NIPAAm]:[DMAEAm]:[mCTA]:[Initiator] ratios of 18:18:1:0.1 were used in MeOH. MeOH was chosen because the mCTA was highly soluble in MeOH. The diblock copolymer ((2) in Figure 2) was found to have a M_n=17.7 by MALS, PDI=1.25, and dn/dc=0.071. GPC traces of the mCTA and the diblock copolymer can be found in the Supporting Information (Figure S1). ^{1}H-NMR of the diblock copolymer can be found in the Supporting Information (Figure S2). ^{1}H-NMR results from diblock copolymer preparations showed that the chemical shift of the DMAEAm methyl group protons was dependent on the protonation state of the tertiary amine. Diblock copolymers treated with 10 equivalents of NaOH to deprotonate the amines of DMAEAm were found to have DMAEAm methyl group shifts at δ (ppm)=2.26 (s, R-N($C\underline{H}_3$)$_2$. Polymers treated with 10 equivalents of HCl prior to NMR analysis, however, were found to have DMAEAm methyl group shifts at δ (ppm)=3.1 (s, R-N($C\underline{H}_3$)$_2$. Previous studies have reported the proton shift of the DMAEAm methyl group in monomeric form to be δ (ppm)=2.26 (24). In analyzing Figure S2, the four protons located between the amide and tertiary amine groups of DMAEAm were also assigned to the peak at δ (ppm)=3.1, which therefore represented 10 DMAEAm protons. The DPN of DMAEAm in the diblock was ~15, based on the 1:1.15 integrated peak area ratio of the single NIPAAm hydrogen at δ (ppm)=4.0 to the 10 DMAEAm protons at δ (ppm)=3.1. The overall NIPAAm:DMAEAm ratio in the diblock copolymer was ~9:1.

Biotinylation of diblock copolymer

The 17.7 kDa diblock copolymer was biotinylated via DCC/NHS ester activation and conjugation to NH_2-PEG_2-biotin. The dicyclohexylurea byproduct was removed using a 0.2 μm syringe filter. Biotinylation efficiency was measured by commercially available HABA dye-displacement assay (25). Known amounts of polymer were added to a solution of HABA-saturated avidin. The decrease in absorbance at 500 nm due to HABA dye displacement from the binding pocket was measured. A standard curve generated by addition of variable amounts of free biotin to the HABA-saturated avidin was used as a reference to quantify the number of available biotin moieties in the polymer preparations. The biotinylation efficiency was found to be 78% for the 17.7 kDa diblock copolymer. Results from the HABA dye displacement assay can be found in the Supporting Information (Figure S3).

Nanoparticle synthesis and characterization

Citrate-stabilized gold nanoparticles were synthesized using a protocol from the literature (23). Within 3 minutes of addition of sodium citrate to the boiling gold chloride solution, a rapid color change from yellow to deep red was observed. The positively charged diblock copolymer was allowed to interact with the negatively charged citrate-capped AuNPs overnight. In addition to electrostatics, chemisorption of the trithiocarbonate group from the RAFT CTA likely contributes to successful modification of the AuNPs (26). The polymer-modified AuNPs were then successfully transferred into 3 mL of 1x PBS buffer using membrane ultrafiltration. The AuNPs were washed off of the cellulose membrane and remained soluble for months stored in PBS buffer under N_2 at 4 °C. AuNPs were characterized by TEM imaging, particle sizing image analysis, and absorption spectrophotometry (Figure 3, top panel A–C). From TEM images, the AuNPs had pseudo-spherical morphology with diameter = 23.5 ± 4.28 nm (mean ± standard deviation, # of particles counted > 200). The LSPR absorption peak (Figure 3, C) was observed at 530 nm. The extinction coefficient of the 23 nm AuNPs was estimated to be $2*10^9$ $M^{-1}cm^{-1}$ from sizing data and the literature (27). This molar extinction coefficient was used in further studies to estimate the concentration of the AuNPs.

Unlike citrate-stabilized AuNPs, the polymer-modified AuNPs were found to be colloidally stable in physiological buffers (e.g., PBS). The localized surface plasmon resonance (LSPR) wavelength did not red-shift after transfer of the particles into PBS buffer. The LSPR wavelength of the AuNPs was red-shifted upon raising the temperature above the LCST of the polymer (Figure 4C & D). Below the LCST, the gold colloid had an absorption peak at 530 nm, and transmitted white light appears pink (Figure 4C). After raising the temperature above the LCST, the LSPR was red-shifted by ~40 nm and the solution appeared purple (Figure 4D). The color change is due to dielectric coupling of LSPR oscillations between aggregated AuNPs in close proximity to each other (28). This behavior is similar to what has been previously reported on “smart” polymer-AuNP conjugates (29–33). Interestingly, the red-shift of the LSPR was prevented upon addition of 0.2 mg/mL of homo-pNIPAAm free polymer. Addition of free polymer insulates the AuNPs from one another, preventing them from becoming sufficiently close in proximity to allow for coupling of the LSPR.

The mNPs were synthesized using a 5-kDa homo-pNIPAAm, as previously described (4). This homo-pNIPAAm served as a stabilizer during mNP synthesis, resulting in pNIPAAm-coated mNPs. TEM and particle size analysis of the mNPs (Figure 3D and 3E) showed they have an average long-axis diameter of 9.1 ± 2.44 nm (mean ± standard deviation, # of particle counted > 60). The optical absorption spectrum of the mNPs shows a Rayleigh scattering profile, as seen in Figure 3F. The mNPs exhibit a thermally triggered increase in the magnetophoretic mobility, as has been previously described (4,5,34,35). This behavior is

demonstrated in Figure 4, A and B. Below the LCST (Figure 4A), the mNPs do not rapidly respond to the magnet placed against the side of the cuvette because they exist as the <10 nm particles. When the temperature is raised above the polymer LCST (Figure 4B), the large aggregates have much larger magnetophoretic mobility, and are rapidly separated against the cuvette side-wall by the magnet.

Both particle types (AuNPs and mNPs) therefore exhibit thermally-triggered aggregation that modulates their magnetic and/or optical properties. It was found that mixtures of these two particle types possessed both the magnetic separation behavior of the mNPs combined with the optical extinction properties of the AuNPs. AuNPs modified with the diblock copolymers could therefore be magnetically separated upon co-aggregation with the pNIPAAm-coated mNPs and application of a magnetic field gradient. Video stills demonstrating magnetic separation of AuNPs can be found in the Supporting Information (Figure S4).

Magnetic Enrichment of Alexafluor®-750-Labeled Streptavidin

As a validation of the bioseparation technique, we tested the ability of AuNPs to bind fluorescently labeled streptavidin, and concentrate the target protein via polymer-induced co-aggregation and magnetic separation with mNPs. An advantage of this nanoparticle system is the ability to process large sample volumes as easily as μL quantities. This capability was demonstrated by increasing the total processed sample volume at a fixed concentration of labeled streptavidin. AF-750 streptavidin (5 nM) spiked into 50% human plasma was used to mimic a clinical sample. 3 nM of diblock-copolymer-modified AuNPs, 2 mg/mL mNPs, and 2 mg/mL of 8 kDa homo-pNPAAm were added sequentially. Each AuNP is expected to bind no more than 50 streptavidin molecules based on nanoparticle size and a theoretical streptavidin monolayer density of 2.8 ng/mm^2 (36).

Samples of 100, 250, or 500 μL were heated to 45 °C causing polymer collapse and mixed AuNP/mNP aggregate self-assembly. A magnet was applied, and the aggregates were captured at the side of the carrying vessel. The supernatant was discarded, and the captured pellet was redissolved into a 10 μL volume of cool (<LCST) PBS 6.0 buffer. Figure 5 shows fluorescence and absorbance measurements taken on the redissolved aggregates below the LCST. Data bars in Figure 5 represent mean ± SD (n=5) of labeled-streptavidin fluorescent intensity at 776 nm, or particle absorbance at 520 nm. Increasing the sample volume results in a corresponding linear increase in the AuNP absorbance and streptavidin fluorescence. In the presence of free biotin, the streptavidin binding sites are blocked and fluorescence capture is eliminated, demonstrating that capture is occurring via specific streptavidin-biotin binding. Only a small amount of fluorescence is captured due to non-specific adsorption of the labeled-streptavidin to the nanoparticle/polymer aggregates.

LFIA Device Fabrication

We further demonstrated the capabilities of the bioseparation/enrichment system by developing a quantitative lateral flow immunoassay of the model protein analyte streptavidin. LFIA strips were fabricated using and in-house protein striping system capable of depositing the capture antibody (rabbit polyclonal anti-streptavidin IgG) within the confines of a narrow line ~1.5 mm in width onto nitrocellulose substrates. The nitrocellulose strips and absorbent wicking pads were placed onto adhesive-coated mylar. An image of the lateral flow strip can be seen in Figure 6, top.

Effect of Streptavidin Dose on LFIA Signal

Figure 6 shows the light extinction signal generated by processing varying amounts of streptavidin from 200 μL sample volumes, and flowing the resuspended particle mixtures

through the capture antibody line on the LFIA strips, followed by a rinse step. The curve is linear with a limit of detection of 6 ng/mL, determined using 3 times the standard error of the zero antigen sample as the lower signal limit. The dual AuNP/mNP nanoparticle system is therefore able to generate specific signal proportional to the amount of diagnostic target in the sample, facilitating quantitative assays when combined with optical reader technologies.

Effect of Concentrating Model Biomarker from a Larger Sample Volume on LFIA Signal

By increasing the volume of the sample processed at a fixed concentration of streptavidin, we effectively capture more molecules of the target protein, which translates into increased light extinction at the test line of the LFIA strip. Figure 7 shows the increase in LFIA signal that was accomplished by increasing the sample volumes from 100–500 μL for a fixed 10 ng/mL of streptavidin. A 500 μL sample without streptavidin (500, 0 SA) served as the negative control. These results demonstrate that the smart nanoparticle system can increase the signal at a fixed analyte concentration by processing larger volumes of sample. Where larger samples can be obtained from the patient, this finding has implications for opening up new biomarkers to point-of-care testing that are currently too dilute to be detected by conventional non-concentrating LFIA.

DISCUSSION

These results demonstrate the possibility of enhancing the performance of rapid tests using the dual AuNP/mNP system to achieve rapid and integrated biomarker labeling, purification, enrichment, and detection. Our key innovation was using stimuli-responsive coatings to direct co-aggregation of two different types of nanoparticles, each with pre-designed functionalities. The mNPs enable separation/enrichment of the diagnostic target bound to the AuNPs when the aggregate size is large enough to achieve rapid magnetophoretic separations, while the AuNPs provide a high-efficiency absorbing species by which the target molecule is visualized without the need for advanced optical instrumentation. One advantage of the dual particle system over a magnetic-core/gold-shell nanoparticle system is the ability to independently control the stoichiometric ratios of the magnetic and gold particles. This allows optimization of each particle type independent from one another, and also facilitates tuning the magnetophoresis behavior. For example, when magnetophoresis is found to be slow, more magnetic particles can be added to improve the separation without changing the amount of gold nanoparticles in the mixture. Future work will focus on transferring these proof-of-concept results to a real biomarker system by incorporating capture antibodies onto the AuNPs for disease-related and multiplexed antigen detection from clinical samples.

Supplementary Material

Refer to Web version on PubMed Central for supplementary material.

Acknowledgments

Michael A. Nash gratefully acknowledges funding from the National Science Foundation Graduate Research Fellowship Program (NSF-GRFP), and from the U.S. Department of Homeland Security (DHS) Scholarship and Fellowship Program, administered by the Oak Ridge Institute for Science and Education (ORISE) through an interagency agreement between the U.S. Department of Energy (DOE) and DHS. Dr. Selvi Srinivasan is acknowledged for helpful discussions on NMR. This work was supported in part by funding from the National Institutes of Health (Grant EB000252), and The Bill and Melinda Gates Foundation through the Grand Challenges Program.

References

1. Posthuma-Trumpie GA, Korf J, van Amerongen A. Lateral flow (immuno) assay: its strengths, weaknesses, opportunities and threats. A literature survey. Analytical and Bioanalytical Chemistry. 2009; 393:569–582. [PubMed: 18696055]
2. Gordon J, Michel G. Analytical Sensitivity Limits for Lateral Flow Immunoassays. Clinical Chemistry. 2008; 54:1250–1251. [PubMed: 18593968]
3. Anderson NL, Polanski M, Pieper R, Gatlin T, Tirumalai RS, Conrads TP, Veenstra TD, Adkins JN, Pounds JG, Fagan R, Lobley A. The human plasma proteome - A nonredundant list developed by combination of four separate sources. Molecular & Cellular Proteomics. 2004; 3:311–326. [PubMed: 14718574]
4. Lai JJ, Hoffman JM, Ebara M, Hoffman AS, Estournes C, Wattiaux A, Stayton PS. Dual magnetic-/temperature-responsive nanoparticles for microfluidic separations and assays. Langmuir. 2007; 23:7385–7391. [PubMed: 17503854]
5. Lai JJ, Nelson KE, Nash MA, Hoffman AS, Yager P, Stayton PS. Dynamic bioprocessing and microfluidic transport control with smart magnetic nanoparticles in laminar-flow devices. Lab on a Chip. 2009; 9:1997–2002. [PubMed: 19568666]
6. Zhao W, Brook MA, Li YF. Design of gold nanoparticle-based colorimetric biosensing assays. Chembiochem. 2008; 9:2363–2371. [PubMed: 18821551]
7. Zhao W, Ali MM, Aguirre SD, Brook MA, Li Y. Paper-based bioassays using gold nanoparticle colorimetric probes. Analytical Chemistry. 2008; 80:8431–8437. [PubMed: 18847216]
8. Wilson R. The use of gold nanoparticles in diagnostics and detection. Chemical Society Reviews. 2008; 37:2028–2045. [PubMed: 18762845]
9. Shyu RH, Shyu HF, Liu HW, Tang SS. Colloidal gold-based immunochromatographic assay for detection of ricin. Toxicon. 2002; 40:255–258. [PubMed: 11711121]
10. Dar VS, Ghosh S, Broor S. Rapid Detection of Rotavirus by Using Colloidal Gold Particles Labeled with Monoclonal-Antibody. J Virol Methods. 1994; 47:51–58. [PubMed: 8051233]
11. Kunakorn M, Petchclai B, Khupulsup K, Naigowit P. Gold Blot for Detection of Immunoglobulin-M (IgM)-Specific and IgG-Specific Antibodies for Rapid Serodiagnosis of Melioidosis. J Clin Microbiol. 1991; 29:2065–2067. [PubMed: 1723079]
12. Hsu YH. Immunogold for Detection of Antigen on Nitrocellulose Paper. Analytical Biochemistry. 1984; 142:221–225. [PubMed: 6083735]
13. Brada D, Roth J. Golden Blot-Detection of Polyclonal and Monoclonal-Antibodies Bound to Antigens on Nitrocellulose by Protein-A Gold Complexes. Analytical Biochemistry. 1984; 142:79–83. [PubMed: 6083736]
14. Nash MA, Lai JJ, Hoffman AS, Yager P, Stayton PS. “Smart” Diblock Copolymers as Templates for Magnetic-Core Gold-Shell Nanoparticle Synthesis. Nano Letters. 2010; 10:85–91. [PubMed: 20017498]
15. Bardhan R, Chen WX, Perez-Torres C, Bartels M, Huschka RM, Zhao LL, Morosan E, Pautler RG, Joshi A, Halas NJ. Nanoshells with Targeted Simultaneous Enhancement of Magnetic and Optical Imaging and Photothermal Therapeutic Response. Advanced Functional Materials. 2009; 19:3901–3909.
16. Xu ZC, Hou YL, Sun SH. Magnetic core/shell Fe3O4/Au and Fe3O4/Au/Ag nanoparticles with tunable plasmonic properties. Journal of the American Chemical Society. 2007; 129:8698. [PubMed: 17590000]
17. Lim IIS, Njoki PN, Park HY, Wang X, Wang LY, Mott D, Zhong CJ. Gold and magnetic oxide/gold core/shell nanoparticles as bio–functional nanoprobes. Nanotechnology. 2008; 19:11.
18. Park HY, Schadt MJ, Wang L, Lim IIS, Njoki PN, Kim SH, Jang MY, Luo J, Zhong CJ. Fabrication of magnetic core @ shell Fe oxide @ Au nanoparticles for interfacial bioactivity and bio-separation. Langmuir. 2007; 23:9050–9056. [PubMed: 17629315]
19. Lyon JL, Fleming DA, Stone MB, Schiffer P, Williams ME. Synthesis of Fe oxide core/Au shell nanoparticles by iterative hydroxylamine seeding. Nano Letters. 2004; 4:719–723.
20. Hoffman AS. Bioconjugates of intelligent polymers and recognition proteins for use in diagnostics and affinity separations. Clinical Chemistry. 2000; 46:1478–1486. [PubMed: 10973893]

21. Jassam N, Jones CM, Briscoe T, Horner JH. The hook effect: a need for constant vigilance. Annals of Clinical Biochemistry. 2006; 43:314–317. [PubMed: 16824284]
22. Moad G, Chong YK, Postma A, Rizzardo E, Thang SH. Advances in RAFT polymerization: the synthesis of polymers with defined end-groups. Polymer. 2005; 46:8458–8468.
23. Frens G. Controlled nucleation for regulation of particle-size in monodisperse gold suspensions. Nature-Physical Science. 1973; 241:20–22.
24. Chen TM, Wang YF, Kitamura M, Nakaya T, Sakurai I. Synthesis and properties of poly(acrylamide)s containing both long chain alkyl groups and phosphatidylcholine analogues in the side chains. Journal of Polymer Science Part a-Polymer Chemistry. 1996; 34:1155–1164.
25. Green NM. A spectrophotometric assay for avidin and biotin based on binding of dyes by avidin. Biochemical Journal. 1965; 94:C23.
26. Fustin CA, Duwez AS. Dithioesters and trithiocarbonates monolayers on gold. Journal of Electron Spectroscopy and Related Phenomena. 2009; 172:104–106.
27. Haiss W, Thanh NTK, Aveyard J, Fernig DG. Determination of Size and Concentration of Gold Nanoparticles from UV-Vis Spectra. Analytical Chemistry. 2007; 79:4215–4221. [PubMed: 17458937]
28. Jain PK, Huang WY, El-Sayed MA. On the universal scaling behavior of the distance decay of plasmon coupling in metal nanoparticle pairs: A plasmon ruler equation. Nano Letters. 2007; 7:2080–2088.
29. Aqil A, Qiu HJ, Greisch JF, Jerome R, De Pauw E, Jerome C. Coating of gold nanoparticles by thermosensitive poly(N-isopropylacrylamide) end-capped by biotin. Polymer. 2008; 49:1145–1153.
30. Boyer C, Whittaker MR, Luzon M, Davis TP. Design and Synthesis of Dual Thermoresponsive and Antifouling Hybrid Polymer/Gold Nanoparticles. Macromolecules. 2009; 42:6917–6926.
31. Raula J, Shan J, Nuopponen M, Niskanen A, Jiang H, Kauppinen EI, Tenhu H. Synthesis of gold nanoparticles grafted with a thermoresponsive polymer by surface-induced reversible-addition-fragmentation chain-transfer polymerization. Langmuir. 2003; 19:3499–3504.
32. Yusa SI, Fukuda K, Yamamoto T, Iwasaki Y, Watanabe A, Akiyoshi K, Morishima Y. Salt effect on the heat-induced association Behavior of gold nanoparticles coated with Poly(N-isopropylacrylamide) prepared via reversible addition - Fragmentation chain transfer (RAFT) radical polymerization. Langmuir. 2007; 23:12842–12848. [PubMed: 17994778]
33. Zhu MQ, Wang LQ, Exarhos GJ, Li ADQ. Thermosensitive gold nanoparticles. Journal of the American Chemical Society. 2004; 126:2656–2657. [PubMed: 14995155]
34. Furukawa H, Shimojyo R, Ohnishi N, Fukuda H, Kondo A. Affinity selection of target cells from cell surface displayed libraries: a novel procedure using thermo-responsive magnetic nanoparticles. Applied Microbiology and Biotechnology. 2003; 62:478–483. [PubMed: 12750854]
35. Sun YB, Ding XB, Zheng ZH, Cheng X, Hu XH, Peng YX. Magnetic separation of polymer hybrid iron oxide nanoparticles triggered by temperature. Chemical Communications. 2006:2765–2767. [PubMed: 17009456]
36. Gau JJ, Lan EH, Dunn B, Ho CM, Woo JCS. 2001:745–755.

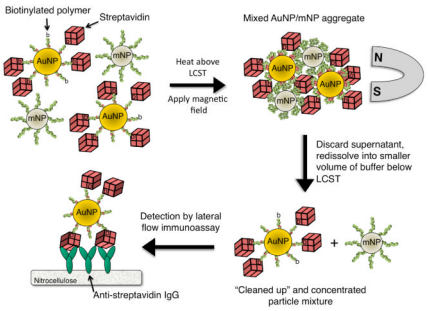

Figure 1.

Dual nanoparticle magnetic separation scheme. AuNPs coated with biotinylated diblock copolymers bind to streptavidin spiked into 50% human plasma. mNPs coated with homo-pNIPAAm are added, and the temperature is raised above the polymer LCST. Mixed streptavidin-AuNP/mNP aggregates are separated by a magnet. The separated aggregates with gold-labeled target protein are resuspended into a smaller volume of buffer below the LCST, and flowed through an LFIA strip with immobilized capture antibodies. Visualization of the target protein is achieved by AuNP light extinction at the capture line of the LFIA strip, while the non-biofunctional mNPs are rinsed away.

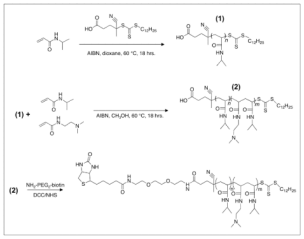

Figure 2.
Diblock copolymerization scheme. The polymer contains a homo-pNIPAAm block (n=130) for thermal responsiveness, a cationic DMAEAm-co-NIPAAm random copolymer block (m=15) to drive adsorption onto anionic AuNPs, and a terminal biotin moiety.

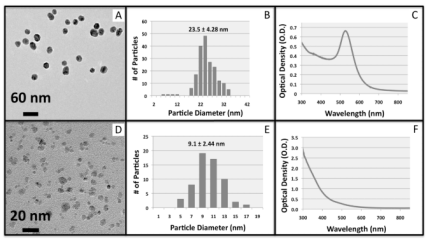

Figure 3.
Characterization of magnetic and gold nanoparticles. TEM images, image analysis particle sizing histograms, and visible absorption spectra of AuNPs (top panel, A–C) and mNPs (bottom panel, D–F).

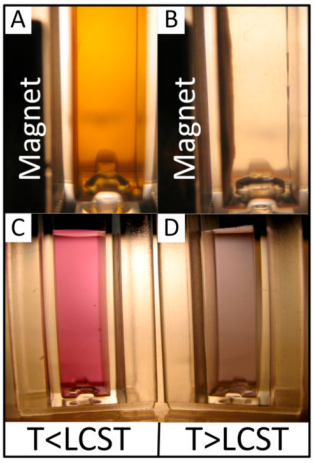

Figure 4.
Photographs of white light transmittance through nanoparticle solutions. mNPs below the polymer LCST (A) do not respond to the magnet, but above the LCST (B) are aggregated and magnetically pulled against the cuvette wall. AuNPs below the LCST (C) appear pink, while above (D) the LCST appear purple due to aggregation and near-field plasmonic coupling.

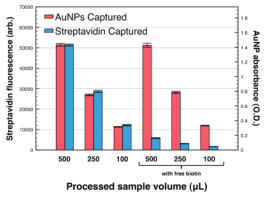

Figure 5.

Magnetic enrichment of fluorescent-streptavidin by AuNP/mNP mixtures. AF-750 labeled-streptavidin fluorescence and AuNP absorbance were measured after processing variable volumes of 50% human plasma containing 5 nM fluorescent-streptavidin. In all cases, the captured particles were redissolved into 10 μL of PBS 6.0 buffer, achieving a 50-fold, 25-fold, or 10-fold particle/protein enrichment factor for the 500, 250, and 100 μL samples, respectively. Samples spiked with 1 μM free biotin served as negative controls to block the streptavidin binding sites preventing fluorescence capture, while particle capture/absorbance remained high.

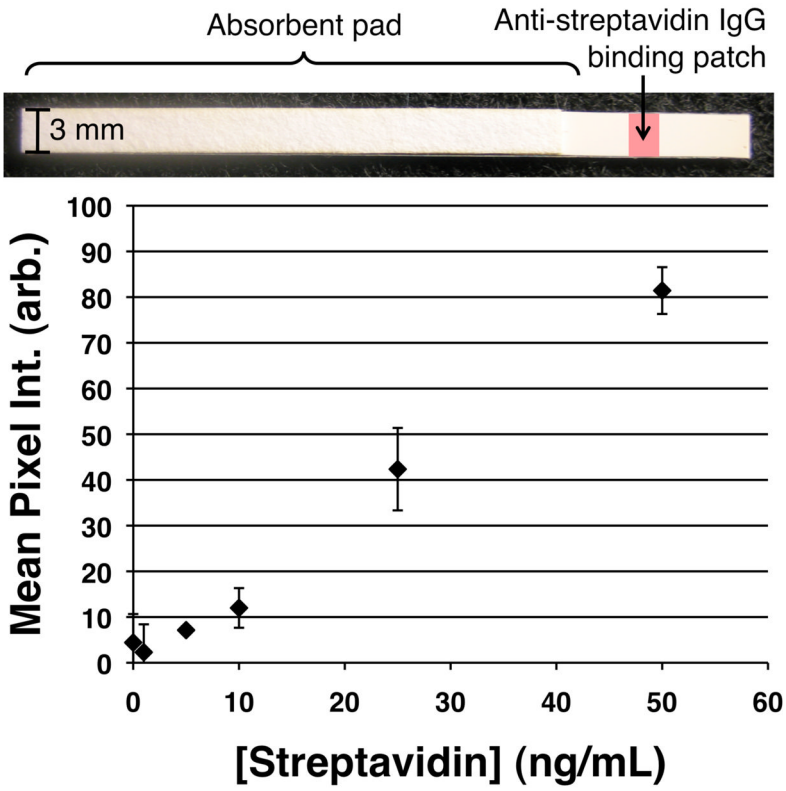

Figure 6.
Lateral flow immunoassay standard curve. (Top) Image of the flow strip. (Bottom) Variable amounts of streptavidin spiked into 50% human plasma samples were captured at a fixed sample volume of 200 μL. The background-subtracted mean pixel intensity (mean ± SD, (n=3)) at the leading edge of the anti-streptavidin IgG binding patch on the nitrocellulose membrane was measured using Image J.

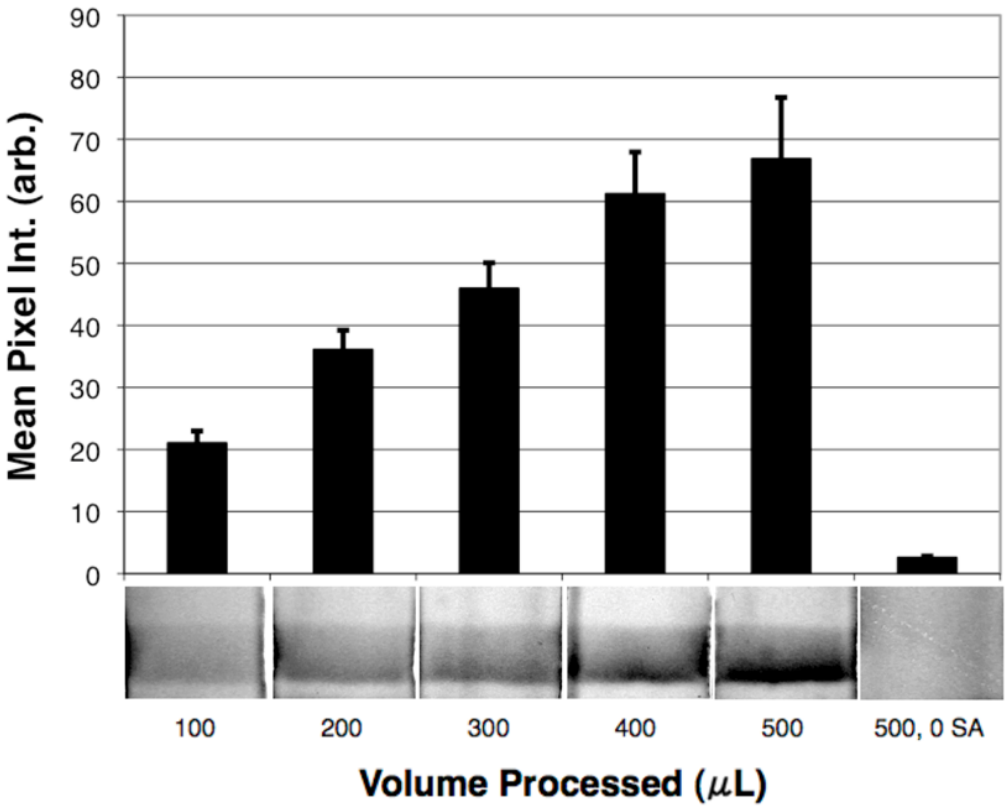

Figure 7.

Effect of increasing sample volume on LFIA signal. Increasing sample volumes from 100–500 μL each with the same concentration of streptavidin (10 ng/mL) were processed using the AuNP/mNP bioseparaton method. 500 μL of 50% human plasma containing the nanoparticle reagents, but no streptavidin (500, 0 SA) served as the negative control.